Published in final edited form as:
Dev Biol. 2013 May 1; 377(1): 224–235. doi:10.1016/j.ydbio.2013.01.014.

C. elegans fmi-1/flamingo and Wnt pathway components interact genetically to control the anteroposterior neurite growth of the VD GABAergic neurons

Elvis Huarcaya Najarro and **Brian D. Ackley***
The Department of Molecular Biosciences, The University of Kansas, Lawrence, KS 66045, United States

Abstract

Directed axonal growth is essential to establish neuronal networks. During the early development of the VD neurons, an anterior neurite that will become the VD axon extends along the anteroposterior (A/P) axis in the ventral nerve cord (VNC) in *Caenorhabditis elegans*. Little is known about the cellular and molecular mechanisms that are important for correct neurite growth in the VNC. In *fmi-1/flamingo* mutant animals, we observed that some postembryonically born VD neurons had a posterior neurite instead of a normal anterior neurite, which caused aberrant VD commissure patterning along the A/P axis. In addition, VD anterior neurites had underextension defects in the VNC in *fmi-1* animals, whereas VD commissure growth along the dorsoventral (D/V) axis occurred normally in these animals, suggesting that *fmi-1* is important for neurite growth along the A/P axis but not the D/V axis. We also uncovered unknown details of the early development of the VD neurons, indicating that the neurite defects arose during their early development. Interestingly, though *fmi-1* is present at this time in the VNC, we did not observe FMI-1 in the VD neurons themselves, suggesting that *fmi-1* might be working in a cell non-autonomous fashion. Furthermore, *fmi-1* appears to be working in a novel pathway, independently from the planar cell polarity pathway and in parallel to *lin-17/frizzled* and *dsh-1/dishevelled*, to determine the direction of neurite growth. Our findings indicate that redundant developmental pathways regulate neurite growth in the VNC in *C. elegans.*

Keywords

Flamingo; Axon guidance; Neurite growth; Anterior/posterior patterning; Wnt; Frizzled; Dishevelled

Introduction

During the *in vivo* formation of the nervous system, neurons extend axons in a stereotypical manner. Axons grow along the three main axes of development: left–right, dorsoventral (D/V) and anteroposterior (A/P). Failure to do so has deleterious consequences for the formation of neuronal circuits.

*Correspondence to. 5004 Haworth Hall 1200 Sunnyside Ave. Lawrence, KS 66045. Fax: +1 785 8645 821. bdackley@ku.edu. .

Appendix A. Supplementary Information Supplementary data associated with this article can be found in the online version at. http://dx.doi.org/10.1016/j.ydbio.2013.01.014

Correct axonal growth along the A/P axis requires both long-range and short-range cues. Recent observations have implicated Wnt signaling in the formation of neuronal processes along the A/P axis (Hilliard and Bargmann, 2006; Kirszenblat et al., 2011;Lyuksyutova et al., 2003; Pan et al., 2006; Zou, 2006). In *C. elegans*, Wnts provide long-range repellent signals, especially during axon growth and pathfinding (Maro et al., 2009).

While Wnt pathways can provide long-range positional cues, adhesion proteins regulate axon growth and pathfinding more locally (Takeichi, 2007). *fmi-1/flamingo* is a conserved non-classical cadherin that contains multiple protein domains, including nine cadherin repeats and a seven transmembrane domain (Najarro et al., 2012; Steimel et al., 2010). In *C. elegans*, mutations in *fmi-1* cause axon growth and guidance defects along the A/P axis in the ventral nerve cord (VNC) in the pioneer, pioneer follower, HSN and GABAergic neurons (Najarro et al., 2012; Steimel et al., 2010). In different contexts, Flamingo proteins function in both a cell autonomous and a cell non-autonomous fashion (Chen and Clandinin, 2008; Lee et al., 2003; Najarro et al., 2012; Senti et al., 2003; Steimel et al., 2010).

fmi-1 homologs can work as part of the planar cell polarity (PCP) pathway to regulate axon growth and guidance. For example, mutations in *celsr3*, a vertebrate *fmi-1* homolog, cause defects in axon growth and guidance of various neurons along the A/P axis that are similar to those observed when other PCP pathway components are mutated (Fenstermaker et al., 2010; Shafer et al., 2011). Therefore, it appears that in vertebrates, PCP-like pathways control axonal growth and guidance along the A/P axis. It is unknown if similar pathways exist in *C. elegans*.

We study a subset of the D-type GABAergic neurons, the VD neurons. These neurons are born beginning at the late larval 1 stage (L1 stage) in the VNC. A mature, fully differentiated VD neuron contains a ventral axon, a ventrodorsal commissure and a dorsal dendrite, all of which originate from an anterior neurite (AN) (Hall and Russell, 1991; Knobel et al., 1999). Little is known about the molecular and cellular mechanisms that are essential for the directional growth of the AN in the VNC.

We have previously described a set of axon guidance and synaptic defects in GABAergic and cholinergic motoneurons in *C. elegans* animals due to mutations in *fmi-1* (Najarro et al., 2012). Here, we report that *fmi-1* is important for the direction of growth of the AN of the VD neuron. We have observed that some VD neurons in *fmi-1* animals displayed a posterior neurite instead of an AN, causing VD ventrodorsal commissures to be positioned posterior to their cell bodies. We have named this phenotype as the posterior neurite (PN) phenotype. Developmental sequence experiments suggest that these defects arose when VD neurites were initially extending in the VNC. At this time, FMI-1 was present in neighboring axons in the VNC but not in the VD neurons themselves, suggesting that *fmi-1* worked cell non-autonomously to control the direction of neurite growth in the VD neurons. We also show that, in this context, *fmi-1* appeared to work independently from the PCP pathway. Finally, we describe genetic interactions between *fmi-1* and components of a Wnt pathway, including *egl-20/Wnt*, *lin-44/Wnt*, *lin-17/frizzled* and *dsh-1/dishevelled*. Together, these results define a key role for *fmi-1* as well as Wnt signaling in regulating the direction of neurite growth in the VD neurons along the A/P axis in the VNC in *C. elegans.*

Materials and methods

C. elegans strains

All *C. elegans* used were hermaphrodites, and strains were maintained at 20–22.5 °C as described (Brenner, 1974). *lhIs35 [Punc-55::gfp], lhIs36[Punc-55::gfp]* and *lhIs44[Punc-25::mcherry]* were isolated using trimethylpsoralen/UV mutagenesis, and

outcrossed to wild-type (*wt*) six times prior to analyses. The following alleles were used: *fmi-1(tm306)* V, *fmi-1(rh308)* V, *cdh-4(lq83)* III, *prkl-1(ok3182)* IV, *vang-1(ok1142)* X, *lin-17(n671)* I, *dsh-1(ok1445)* II, *lin-44(n1792)* I, *egl-20(n585)* IV, *juIs76[Punc-25::gfp]* II, lhIs35[Punc-55::gfp], lhIs36[Punc-55::gfp], lhIs44[Punc-25::mcherry], juIs145[Pflp-13::gfp].

Molecular biology

The *fmi-1::gfp* (Steimel et al., 2010) was injected into *fmi-1 (tm306);juIs76* animals at 0.5 ng μl^{-1} along with coinjection markers at 10 ng μl^{-1} of *Pstr-1::gfp* and 5 ng μl^{-1} *Pmyo-2::rfp* to generate extrachromosomal arrays named *fmi-1*(+) *line #1* and *fmi-1*(+) *line #2*, respectively. *fmi-1*(+) *line #1 (lhEx269)* was crossed into *fmi-1(tm306);lhIs44* and *dsh-1(ok1445)juIs76;fmi-1 (tm306)* to perform colocalization and rescue experiments, respectively. Constructs to express *fmi-1* cDNA in the pioneer *(Podr-2)*, pioneer follower (*Psra-6*) and cholinergic (*Pacr-2*) neurons are described in (Steimel et al., 2010) and (Najarro et al., 2012), respectively. These constructs were injected into *fmi-1 (tm306);juIs76* animals at three different concentrations, 0.5, 2.0 and 10 ng μl^{-1}, along with 10 ng μl^{-1} of *Pstr-1::gfp* as a coinjection marker. At least two extrachromosomal arrays per injection were generated. The *dsh-1::gfp* (Sanchez-Alvarez et al., 2011) was expressed in *dsh-1(ok1445)* animals carrying either *juIs76 or lhIs44. lin-17::tagRFP* was generated from *lin-17::gfp* (Wu and Herman, 2006) and was injected into *lin-17(n671);fmi-1 (tm306);juIs76* mutant animals at 0.5 ng μl^{-1} with 10 ng μl^{-1} of the *Pstr-1::gfp* coinjection marker to generate *lin-17*(+) *lines #1* to #3. The AS marker was created by expressing *tagRFP* under a *Punc-53* promoter (Stringham et al., 2002). *Punc-53::tagRFP* was injected into *wt* animals at 30 ng μl^{-1} with 5 ng μl^{-1} of the *Pmyo-2::rfp* to generate *lhEx240.* Details of the cloning are available upon request.

Phenotype quantification

PN defects using *juIs76* were scored as follows. Adults were visually separated in six regions (R1 to R6 region) along the A/P axis. Cell body number, commissure number and positions were noted. In *wt* animals, the DD and VD commissures are always located anterior to their somas such that regions R1–R5 each contain three commissures, whereas region R6 typically contains four commissures (occasionally, the VD12 and DD6 commissures fasciculate). If a region expected to have three commissures contained only two commissures, this was scored as a PN defect, as long as we were able to find the mispositioned commissure in the region immediately posterior. Of the total PN defects observed, <4% were found within regions.

The expression pattern of *lhIs35[Punc::55::gfp]* was similar to previous observations (Zhou and Walthall, 1998) except that VD precursor cells were also labeled. GFP was detected in the 13 VD neurons, 11 AS neurons, VA1 and PDB. *Punc-55* activity was highest during L2, and was not detected beyond L4, as reported (Zhou and Walthall, 1998). We scored PNs in L2 animals. We acquired Z sections by confocal microscopy followed by a close examination of the presence or absence of PNs. We did not score defects in the VD1 and VD2 because their cell bodies are located close to each other, so their neurites cannot be visualized individually. VD12 and VD13 have similar resolution constraints. Finally, we used the images to score underextension or gap defects in the VNC. Gaps had to be at least half of the size of a VD cell body (≈15–2.0 μm) to be counted.

Early development of the VD neurons

Using *lhIs35*, we acquired Z-stacks of the early VD neurons by confocal microscopy. The VNC was marked by *Punc-53::tagRFP*, which labels DA motoneurons (and later AS). Late L1 and early L2 animals were picked based on size, then confirmed by examination of the

gonad primordium. Images were acquired on an Olympus FV1000 using multi-tracking parameters and a 60x Plan-apochromat objective. Images were exported to ImageJ for analysis and rotation. To measure the anterior and posterior neurites, an oval/circle was drawn around the cell body in ImageJ. Measurements were made from the center of the circle to the anteriormost and posteriormost tip of the neurite via a straight line.

Statistics

We included different sets of VD neurons in the analysis depending on the marker used. For the *juIs76* marker, *n* represents the total number of scored animals multiplied by eleven, which represents the number of examined VD neurons per animal (VD3–VD13). Similarly, the total number of VD neurons per region was calculated by multiplying the total number of animals scored by the number of neurons in each region. For *lhIs35* and *lhIs36*, *n* represents the total number of scored animals multiplied by nine (VD3–VD11). The chi squared test (χ^2) was used to find statistical significance, with $p<0.05$ considered as significant. Error bars represent standard error of proportion.

In all images presented, anterior is to the left.

Results

Patterning of the GABAergic neurons along the A/P axis in C. elegans

Beginning at L2 and during the later life stages, the cell bodies and commissures of DD and VD neurons can be separated into six different regions along the A/P axis, corresponding roughly to the areas covered by the longitudinal processes of the 6 DD neurons.Fig. 1C shows an example of this pattern using *juIs76*, which is expressed in both DD and VD neurons. Regions 1–5 (R1–5) each contains 1 DD and 2 VD neurons, whereas the most posterior region, region 6 (R6), contains 1 DD and 3 VD neurons. In *wt* animals, the commissure for each neuron is always located anterior to its cell body and is typically found within the boundaries of its respective region (Fig. 1A and C). This pattern is displayed by 99% (*n*=175) of *wt juIs76* animals, suggesting that a robust patterning mechanism or mechanisms is in place. We have used this reliable, natural pattern to detect and score mutations that affect directional neurite growth in the VD neurons.

Abnormal posterior growth of the VD neurites in fmi-1 mutant animals

As described above, *wt* VD neurons project an AN. As a result, VD commissures are always located anterior to their cell bodies in *wt* (Fig. 1A). We observed that in *fmi-1 (tm306);juIs76* animals, VD neurons sometimes displayed PNs, causing VD commissures to be positioned on the posterior side of their cell body, which in turn caused a deviation from the pattern described above (Fig. 1B,D,E). For example, in Fig. 1D, VD4 displays a PN. As a consequence, the VD4 commissure is present in region R3 instead of in region R2. As a result, regions R2 and R3 now contain two and four commissures, respectively. In contrast, regions R2 and R3 in control animals always contain three commissures each (Fig. 1C). Further analysis indicated that these defects were not accompanied by either a change in the total number of cell bodies or commissures (Table S1). In addition, the final position of the cell bodies along the A/P axis in adult animals was grossly similar to *wt* (Fig. 1C and D). 2.27% (*n*=2200) of VD neurons in *tm306* animals displayed a PN phenotype (Fig. 1F) and they were found throughout the length of the animal (Fig. 1G). We confirmed these observations with another *fmi-1* loss-of-function (LOF) allele, *fmi-1 (rh308)* (Fig. 1F) (Steimel et al., 2010). We also examined the position of the DD commissures using a DD specific marker, *Pflp-13::gfp*, but we did not see differences between *wt* and *fmi-1* animals (0% PN, *n* = 600 per genotype). These data suggest that in *fmi-1* animals, VD neurons

project PNs that cause aberrant distribution of the VD commissures along the A/P axis. Furthermore, DD neurons in *fmi-1* animals do not display PN defects.

We have previously reported that mutations in *cdh-4* cause patterning defects in VD neurons. We examined *cdh-4(lq83)* mutants and found that these animal do not display PN defects (0% PN, n=1650). Further, there was no significant difference in the penetrance of PN defects in *fmi-1;cdh-4* double mutants (2.41% PN, n=1904) relative to *fmi-1* single mutants (2.27% PN, χ^2 test, p-=0.18). These results indicate that *fmi-1* is likely to function independent of *cdh-4* for A/P neurite outgrowth.

juIs76 labels both DD and VD neurons, making it difficult to visualize individual VD neurites. Therefore, in order to find more evidence for the PN phenotype, we engineered another fluorescent VD marker, *lhIs35 (Punc-55::gfp)* (Fig. 2A). This marker labels two sister cells, VD and AS neurons. AS neurons do not project long ventral neurites, and therefore do not interfere with the quantification of PNs in VD neurons. In agreement with our previous results, 5.34% of VD neurons in L2 *fmi-1* animals displayed PNs when using the *lhIs35* marker (Fig. 2B). The higher penetrance of PN defects in *fmi-1; lhIs35* animals is likely due to an increased sensitivity in observing posteriorly directed neurites. Not all VD neurons were equally affected by the loss of *fmi-1.* For example, VD3 and VD11 did not display PN defects (Table 1). These results confirm that *fmi-1* mutations affect the direction of neurite growth of VD neurons along the A/P axis. Since we observed the presence of these defects as early as L2 stage, we can also conclude that the neurite defects arose very early during development, most likely at the time when the VD neurites are extending in the VNC (see VD developmental sequence experiments below).

fmi-1;lhIs35 animals also displayed underextension defects in their ANs, causing gaps to appear in the VNC (Fig. S1). In fact, 27.78% (n=469) of VD neurons in L2 *fmi-1* animals displayed gaps in the VNC (Table 2). A few gaps were also observed in control animals (Table 2). This result indicates that *fmi-1* is also important for the full extension of the AN along the A/P axis. In all cases, however, we found that VD neurons did extend a ventrodorsal commissure. Therefore, we concluded that the neurite growth in the D/V axis is not affected by mutations in *fmi-1.*

PN defects do not occur in prkl-1 or vang-1 mutants

We next wondered whether other putative components of the PCP pathway (Sanchez-Alvarez et al., 2011) might also be involved in VD neurite growth. However, we did not detect PN defects in *prkl-1/prickle* and *vang-1/Van Gogh* LOF mutants using *juIs76* (0% PN defects, n=1100 per genotype), results that were confirmed using the *Punc-55::gfp* marker (Table 1). We also examined double mutant combinations of *fmi-1* with these two genes. Although PN defects were observed in these animals, we could not confidently score PN defects because of extensive cell positioning defects. We partially overcame this problem by scoring PN defects in region R6 in animals with normal cell positioning. There was no increase in the number of animals displaying PNs in *fmi-1;prkl-1* (0.78% PN, n=510) or *fmi-1;vang-1* (1.33% PN, n=450) compared to *fmi-1* (1.67% PN, n=600) (χ^2 test, p=0.19 and p=0.66, respectively). Thus, *fmi-1* might be working independently from the PCP pathway to control directional neurite growth of the VD neurons.

Overall, these data indicate that *fmi-1* influences the direction of VD neurite growth along the A/P axis in the VNC. When *fmi-1* is mutated, VD neurons display a PN phenotype. In addition, normal, anteriorly - directed VD neurites sometimes fail to fully extend along the A/P axis. Finally, two core components of the PCP pathway do not appear to contribute to the PN phenotype.

Neuroblast division and VD specification are normal in fmi-1 mutants

fmi-1 plays a minor role in asymmetric cell division (Wu and Herman, 2006). We investigated whether the defects present in *fmi-1* animals were due to a failure in asymmetric cell division of the VD precursors. To test this, we used the *lhIs35* marker to label both VDs and their sisters, the AS neurons. By cell morphology, VD neurons were always found posterior to the AS neurons in the VNC in *wt* (Zhou and Walthall, 1998) and *fmi-1* animals (50 animals per genotype). In addition, the total number of cell bodies remained unchanged in these animals (50 animals per genotype). A similar pattern was observed in combination with another AS marker (*Punc-53::tagRFP*) (Fig. 3). These observations suggest that mutations in *fmi-1* do not affect asymmetric cell division as measured by the relative position of sister cells and number of cell bodies.

Given that *lhIs35* expression, along with two other VD differentiation markers, *juIs76* and *oxIs12* (McIntire et al., 1997) (data not shown), were unchanged in *fmi-1* mutant animals, we ruled out VD cell fate errors as a possible cause of the PN defects. Furthermore, the expression of the AS fluorescent marker was not changed in the AS neurons (Fig. 3C and D), indicating that both daughters of the precursor cell expressed lineage-specific markers. Overall, these data suggest that VD neurite defects are unlikely to be due to problems in asymmetric cell division or cell fate specification.

fmi-1 might function cell non-autonomously to regulate directional VD neurite growth

We next performed transgene-mediated rescue experiments. A GFP-labeled version of *fmi-1* driven by its endogenous promoter was able to fully rescue the PN phenotype present in *fmi-1* animals (n=2 lines) (Fig. 4). The VD motoneurons develop during the late L1 and early L2 larval stages (Knobel et al., 1999) (see also VD developmental sequence described below). We used the GFP-labeled FMI-1 to investigate the distribution of FMI-1 at the same time that VD neurites are undergoing neurite extension (Fig. 5). To do this, we outcrossed one of our *fmi-1* rescuing arrays (*lhEx269*) into *fmi-1* animals expressing a red VD marker (*lhIs44*). FMI-1::GFP was detected in the VNC in early L1s, and was therefore present prior to the birth of the VD neurons (not shown). At early L2 stage, when VD neurons are forming their ANs, the FMI-1 protein was consistently present along the VNC (Fig. 5A). It was also present in a punctate pattern along the membrane in the cell bodies of the PVP pioneer and PVQ follower neurons and the cholinergic neurons (not shown). However, we did not observe *fmi-1* expression in the VD neurons (n=25 animals) (Fig. 5C). This expression pattern is consistent with previous reports (Najarro et al., 2012; Steimel et al., 2010). In addition, we were unable to rescue the PN phenotype by expression of FMI-1 specifically in the DD and VD neurons (n=6 lines). Since we can rescue the PN phenotype in *fmi-1* animals with the *fmi-1* promoter, which is not active in the VD neurons, these data suggest that *fmi-1* is likely working cell non-autonomously to regulate directional neurite growth of the VD neurons in the VNC. However, we cannot completely rule out that *fmi-1* is being expressed in the VD neurons at undetectable levels.

Since we observed consistent expression of *fmi-1* in the VNC and because *fmi-1* defects are primarily observed there, we wondered if expression of *fmi-1* cDNA in specific cell populations in the VNC could rescue the PN phenotype. However, we were unable to rescue the PN phenotype present in VD neurons when *fmi-1* was expressed specifically in the AVG, the PVP pioneer neurons, PVQ pioneer follower neurons and the cholinergic neurons, all of which have axons that contribute to the VNC (Fig. S2). We concluded that expression of *fmi-1* in these neurons is not sufficient to rescue the PN defects in *fmi-1* animals.

lin-17 functions in parallel to fmi-1 in region 6

A previous study has shown that a canonical Wnt signaling pathway is important for axon growth and pathfinding of the GABAergic neurons in the dorsal nerve cord (DNC) along the A/P axis in *C. elegans* (Maro et al., 2009). We have found that *fmi-1* interacts genetically with components of the Wnt pathway, including *lin-17/frizzled* and *dsh-1/dishevelled* (Fig. 6, Fig. 7). In *lin-17;juIs76* animals, we found that 1.62% (n=2101) of VD neurons in *lin-17* animals displayed a PN (Fig. 6C). Unlike *fmi-1* mutants, these defects were predominantly observed in the R6 region (Fig. 7A, Fig. S3).

We next performed epistasis analysis between *lin-17* and *fmi-1.* We observed a statistically significant increase in the penetrance of PNs in R6 from 5.93 and 1.67% in *lin-17* and *fmi-1*, respectively, to 17.21% (n=366) in *lin-17;fmi-1* double mutants (Fig. 7A). Double mutant animals also displayed a significant increase in the penetrance of PN defects in R5 (Fig. S3). These results suggest that *lin-17* and *fmi-1* are working in parallel pathways to regulate the direction of neurite growth of the VD neurons located in the posterior side of the animal.

Because *lin-17* can act as a receptor for the Wnt ligands *lin-44* and *egl*-20 (Kirszenblat et al., 2011; Maro et al., 2009), we created double mutant combinations of *fmi-1* with these two genes. *fmi-1*; *lin-44* animals displayed a significant increase in the penetrance of PN defects in the R2 and R6 regions when compared to *fmi-1* animals (Fig. 7C, Fig. S3), whereas *fmi-1*; *egl*-20 animals showed an increase in the penetrance of PN defects in R2–R5 regions (Fig. 7D, Fig. S3). We also observed PN defects in *lin-44* and *egl-20* single mutant animals (Fig. 7C,D). We concluded that *lin-44* and *egl-20* are also acting in parallel to *fmi-1* to regulate the direction of neurite growth of the VD neurons in a context-dependent manner.

The R6 region in *lin-17* animals also displayed other types of defects including cell positioning defects and missing cell bodies (data not shown). Although these defects primarily affected VD11 and VD12, we were concerned that these defects might affect the interpretation of our data. Therefore, we calculated the penetrance of the PN phenotype only in *lin-17* and *lin-17;fmi-1* animals that lacked these types of defects in R6. In agreement with our previous observations, we found a significant increase (χ^2 test, p=0.023) in the penetrance of the PN phenotype in the double mutant compared to the single mutant, 16.36% (n=165) versus 7.58% (n=132), respectively. These results suggest that the observed increase in PNs occurred independently from the other defects present in *lin-17.*

lin-17;lhIs35 animals also displayed the PN phenotype on the posterior side of animals (Table 1). We did not score PN defects in VD13 because the aberrant neurites overlapped with the axon from the PDB neuron, which is also labeled by *lhIs35*, preventing us from confidently scoring these defects. *lin-17* animals also had gaps in the VNC (Table 2; Fig. S1). This result suggests that *lin-17* is also important for directional neurite growth of the VD neurons.

We next performed rescue experiments in the *lin-17;fmi-1* double mutant using a tagRFP-labeled LIN-17, expressed under its endogenous promoter. We were able to fully rescue the PN phenotype in these animals (n=3 lines). In these lines, LIN-17::tagRFP was present in the cell body and neurites of the VD neurons, suggesting that *lin-17* is possibly acting cell autonomously (Fig. 8). However, since we used the endogenous *lin-17* promoter, LIN-17::tagRFP was also present in other parts of the animal including neurons, muscles and epithelium (Fig. 8). Overall, these experiments suggest that *lin-17* works in parallel to *fmi-1* to control the direction of neurite growth of the VD neurons in the R6 region.

dsh-1 is a genetic enhancer of fmi-1

We next analyzed the interaction between *fmi-1* and *dsh-1* (Figs. 6 and 7B). Double mutants of *fmi-1* with *dsh-1* showed a statistically significant increase in the penetrance of the PN phenotype. In fact, 5.73% (n=1100) of VD neurons in *fmi-1;dsh-1juIs76* animals had PNs, whereas, as described above, only 2.27% of *fmi-1;juIs76* VD neurons had these defects (Fig. 7B). Unlike the genetic interaction of *fmi-1* with *lin-17*, we observed an increase in the penetrance of the PN phenotype throughout the length of the animal. We confirmed these results by looking at *dsh-1;fmi-1;lhIs35* animals (Table 1; Fig. 9). Transgenic expression of *fmi-1* was able to fully rescue the PN phenotype in the *dsh-1;fmi-1* double mutant (Fig. 7B). These data suggest that *dsh-1* is a genetic enhancer of *fmi-1.*

Surprisingly, we did not find PN defects in the *dsh-1* single mutant using either *juIs76* or *lhIs35.* However, a small number of *dsh-1* animals (10–15%) displayed defects in the growth of the dorsal neurites in R6 region (Fig. 6D). In addition, *dsh-1;lhIs35* animals displayed underextension defects or gaps in the VNC like those observed in *fmi-1* mutants (Table 2; Fig. S1). The numberand position of the VD cell bodies appear to be normal in *dsh-1;lhIs35* animals (Fig. S1).

We next performed colocalization experiments to find out if *dsh-1* is expressed in the VD neurons. We observed colocalization of a *dsh-1* genomic DNA fragment fused to *gfp* with a red VD marker (Fig. 10). *DSH-1*::GFP was present in the cytoplasm of the VD neurons during early L2 stage with no obvious asymmetric localization (Fig. 10). In addition, expression of this transgene in a *dsh-1juIs76* background caused overextension defects in the DNC in the R6 region (Fig. S4). These experiments indicate that *dsh-1* is expressed in the VD neurons and that it could be acting cell autonomously in parallel to *fmi-1* to regulate the direction of neurite growth. Furthermore, over expression of *dsh-1* can cause neurite overgrowth on the DNC, suggesting a role for *dsh-1* during neurite growth along the A/P axis. Overall, *dsh-1* appears to work in a parallel pathway to that of *fmi-1* to control the directional neurite growth of the VD neurons.

Mutations in fmi-1 affect A/P neurite growth during early VD development

Our observations suggest that neurite defects in *fmi-1* animals arise during the early development of the VD neurons. Using *lhIs35*, we examined VD neurons during the neuroblast division through neurite extension stages in both *wt* and *fmi-1;dsh-1* animals (Fig. 11). We used *fmi-1;dsh-1* because these animals have a higher incidence of defects (see above). To confirm our observations, *fmi-1* single mutant animals were also examined. In wt, neuroblasts divided in the A/P axis during L1 (Fig. 11A). We found no differences in *fmi-1* (not shown) or *fmi-1;dsh-1* mutant animals (Fig. 11D) in the timing or orientation of division.

Shortly after division, the lateral aspect of the cell body flattened along the major bundle of the VNC. Then, a neurite process was observed to extend from the anterior part of the flattened lateral aspect where it was contacting the VNC (Fig. 11B) and elongate in the anterior direction, running along the major bundle of the VNC (Fig. 11C). In the *fmi-1;dsh-1* mutants (and *fmi-1*—not shown), VD cells occasionally had a posterior projection from the lateral edge (Fig. 11E), and neurites extending posteriorly (Fig. 11F). It was not uncommon (~15–20% of VDs examined) to observe both anterior and posterior projections in VDs in *wt* animals (Fig. 11G). We measured the lengths of these projections and found that in *wt*, on average, the anterior process was 2.2-fold longer than the posterior (n=12) and only in 1/12 cases was the posterior process longer than the anterior. In *fmi-1;dsh-1* mutants the ratio was 0.86 (n=12) and in 6/12 cases the posterior process was longer than the anterior. It is likely that this gives rise to the PN phenotype in older animals.

Discussion

A fundamental step during the early development of the VD neurons is the polarized anterior growth of a single neurite which differentiates following a developmental program to generate a ventral axon, a ventrodorsal commissure and a dorsal dendrite. All of the processes formed by the VD neurons are located anterior to the cell body, indicating that these neurons must contain systems that detect and process information in terms of their relative position in the animal. Thus, abnormalities in these systems can affect proper neuronal development. VD neurons are inhibitory motor neurons, and each single cell covers a unique segment of the body. Thus, VD neurites that extend posteriorly leave segments of the ventral muscles without inhibitory input. In this study, we have shown that *fmi-1, egl-20/Wnt, lin-44/Wnt, lin-17/frizzled* and *dsh-1/dishevelled* are involved in directional neurite growth in the VD neurons, suggesting that multiple molecular cues contribute to proper VD neurite growth along the A/P axis in the VNC in *C. elegans.*

fmi-1 and neurite growth along the A/P axis

To visualize VD neurite growth in the VNC, we used a VD marker that permitted visualization of the ventral processes. *fmi-1* animals had VD neurons that projected a PN instead of an AN. In spite of being misdirected, these posterior neurites were still able to extend ventrodorsal commissures, which resulted in a different commissure pattern of the D-type GABAergic neurons along the A/P axis. *fmi-1* VD neurites also displayed highly penetrant underextension defects. These results suggest that the loss of *fmi-1* negatively affects neurite growth along the A/P axis, whereas ventrodorsal neurite growth is not affected by *fmi-1* mutations. In contrast, netrin UNC-6 and its receptors, UNC-5 and UNC-40, have been previously shown to guide the VD commissures along the D/V axis (Hedgecock et al., 1990;Norris and Lundquist, 2011). Therefore, VD neurite growth may be mechanistically separated along these two axes of development.

Recent studies have shown that *celsr3*, the vertebrate homologue of *fmi-1*, plays important roles during axon growth and guidance along the A/P axis in the embryonic mouse system (Fenstermaker et al., 2010; Shafer et al., 2011). Similarly, our study reveals that *fmi-1* is important for neurite growth along the A/P axis in *C. elegans*, suggesting a conservation of function across species. However, unlike these previous studies, our data does not support the involvement of two PCP pathway components, *prkl-1* or *vang-1*, in this developmental process in *C. elegans*. We show here that neither *prkl-1* nor *vang-1* LOF alleles displayed a *fmi-1*-like phenotype in the VD neurons. In addition, double mutant combinations of *fmi-1* with either of these two genes did not enhance or suppress the PN defects in the VD neurons. Therefore, it is possible that *fmi-1* might be working in a novel developmental pathway to control neurite growth. This is not the first time that *fmi-1* has been shown to function independently from the PCP pathway. For instance, in *C. elegans*, mutations in *fmi-1* cause axon growth and guidance defects in the pioneer and pioneer follower neurons, whereas neither *prkl-1* nor *vang-1* appears to have a role here (Steimel et al., 2010). Moreover, mutations in *flamingo*, the *Drosophila* ortholog of *fmi-1*, cause axonal defects in the photoreceptor neurons that are not phenocopied by mutations in other components of the PCP pathway (Senti et al., 2003).

Studies on *celsr3* also revealed that this protein could be acting cell autonomously to regulate axon growth and guidance in vertebrate systems (Fenstermaker et al., 2010; Shafer et al., 2011). In contrast, our colocalization data suggest that FMI-1 is not present in the VD neurons, suggesting that *fmi-1* could be acting cell non-autonomously to regulate directional neurite growth in *C. elegans.* In fact, specific expression of *fmi-1* cDNA in the VD neurons was not able to rescue the PN defects, whereas expression of *fmi-1* under a promoter that is inactive in the VD neurons was still able to fully rescue the PN defects in the VD neurons.

The cell non-autonomous function of *fmi-1* has been previously reported in both *C. elegans* and *Drosophila* (Chen and Clandinin, 2008; Najarro et al., 2012; Steimel et al., 2010).

fmi-1 and axon tract formation

How does *fmi-1* control neurite growth in the VD neurons? The VNC in *C. elegans* is comprised of two longitudinal axon tracks that run along the anteroposterior axis. The right and left axon tracks are pioneered by AVG and PVPR axons, respectively (Steimel et al., 2010). Previous studies have shown that axon navigation of later born neurons rely on these pioneer neuron axons (Hutter, 2003; Steimel et al., 2010). For example, mechanical or genetic disruption of the AVG neuron can affect the guidance of various neurons in the VNC, including the DD GABAergic neurons (Durbin, 1987) (Hutter, 2003). Moreover, as described above, a study has shown that pioneer-dependent navigation of follower axons is controlled by *fmi-1* (Steimel et al., 2010). Since VD neurons are born postembryonically, at a time when the pioneer neurons are already present in the VNC, it is possible that the neurite growth defects in the VD neurons are due to a failure in axon track formation. In agreement with this idea, we detected consistent presence of FMI-1 in the right axon bundle during the initial extension of the VD neurite. In addition, our data from the early development of the VD neurons reveals that the AN extends while closely following a marker for the right axon track. In order to know if the AN of the VD neurons use the pioneer axons as guidance for their outgrowth, we transgenically expressed the *fmi-1* cDNA in the AVG and PVP pioneer neurons. However, expression of *fmi-1* in these neurons did not rescue the PN defects in the VD neurons. Similar results were found when *fmi-1* was expressed in the PVQ or cholinergic neurons. Therefore, it is possible that *fmi-1* in these neurons is not sufficient for the normal VD neurite extension. It is also possible that we have not yet found the optimal concentration required to rescue the PN defects in the VD neurons in a cell-specific manner. In fact, there is evidence that tight regulation of protein levels is required for the different functions of *flamingo* in the *Drosophila* model (Berger-Muller and Suzuki, 2011). At this point, it remains to be determined which cell or cells express the *fmi-1* that is important for the direction of growth of the VD neurons.

How can a protein that appears to be evenly distributed in the VNC regulate neurite growth toward a specific direction in a cell non-autonomous fashion? One possible explanation is that *fmi-1*, through the adhesive properties of its cadherin domain, promotes anterior growth of a preexisting VD neurite. In this context, *fmi-1* could be partnering with a protein that is located on the anterior VD neurite to ensure anterior neurite growth. One prediction of this model is that the loss of *fmi-1* will cause underextension defects in the VNC. In fact, we observed extensive underextension defects in the VD neurons. However, this model does not explain the presence of PNs in *fmi-1* VD neurons. Our data from the early development of the VD neurons suggest that in addition to an AN, VD neurons appear to have a small posterior process. Therefore, it is possible that *fmi-1*, in addition to promoting anterior neurite extension, might also inhibit posterior neurite growth. However, we only rarely saw mature *fmi-1* VD neurons containing both an anterior neurite and a posterior neurite. Finally, another possibility is that *fmi-1* is involved in VD neuronal polarity. We are confident that the identification and characterization of genes that work in the *fmi-1* pathway will shed light on the molecular mechanisms of directional neurite growth in the VNC.

Redundant developmental pathways control VD neurite growth along the A/P axis in C. elegans

Mounting evidence indicates that Wnt signaling regulates axon guidance and growth along the A/P axis (Zou, 2006). In *C. elegans*, there are multiple Wnt pathways that play redundant roles during axon growth along the A/P axis (Maro et al., 2009). We have found that *lin-17* and *dsh-1* work in parallel to *fmi-1* to regulate the direction of growth of the VD neurites in

the VNC. Although a mutation in either of these two genes enhanced the PN defect present in *fmi-1* animals, one clear difference between these interactions was that *lin-17;fmi-1* animals displayed PN defects primarily in the R6 region whereas PN defects in *dsh-1;fmi-1* animals were found throughout the animal. *lin-17* can work as a receptor for the *lin-44* and *egl-20* Wnt ligands (Kirszenblat et al., 2011; Maro et al., 2009), which form protein gradients along the A/P axis that can act as repellent signals during neurite growth (Maro et al., 2009). The R6 region coincides with the place where both LIN-44 and EGL-20 proteins are detected in *C. elegans* (Harterink et al., 2011), so this could be the reason why the VD neurons located there are more affected by the loss of *lin-17.* In fact, we found an increase in the penetrance of the PN phenotype in *fmi-1; lin-44* and *fmi-1; egl-20* double mutant animals, the former being more specific to the R6 region.

RMEV and RMED are two GABAergic neurons whose cell bodies are located in the nerve ring in *C. elegans.* They extend a longitudinal neurite along the VNC and DNC, respectively. Previous studies have shown that *dsh-1* is important for the extension of the RMEV and RMED neurites along the A/P axis (Song et al., 2010). Similarly, we have found that *dsh-1* animals display VD neurite defects such as underextension in the VNC and DNC. However, *dsh-1* single mutant animals do not display PN defects on their own. We only saw PN defects in the VD neurons when this mutation is combined with the *fmi-1* mutation. These observations clearly suggest that these two genes work in parallel pathways to regulate directional neurite growth.

As mentioned above, there are multiple Wnt pathways in *C. elegans*, including a canonical one in which *bar-1* gene plays an important role as a co-transcription factor (Korswagen, 2002). Our preliminary data suggest that *bar-1* and *fmi-1* also interact genetically to control neurite growth (E.H.N and B.D.A. unpublished results). It will be important to assay the contribution of other known components of the Wnt signaling pathway during directed neurite growth.

In summary, we have uncovered an important function for *fmi-1* during directional neurite growth of the VD neurons in the VNC. Furthermore, known components of the Wnt pathway contribute to the correct growth of the VD neurites along the A/P axis in the VNC.

Supplementary Material

Refer to Web version on PubMed Central for supplementary material.

Acknowledgments

BDA was supported in part by P20 RR016475 from the INBRE Program of the NCRR and RC1 GM091086 from the NIH. We would also like to thank H. Hutter, M. Herman, H. Fares and A. Colavita for strains and reagents, E. Lundquist for critical reading of the manuscript, J. Kelly for his guidance in statistical analysis, R. Xiao and L. Schrag for technical assistance and S. Mitani for the *tm306* allele. Some strains were provided by the CGC, which is funded by NIH Office of Research Infrastructure Programs (P40 OD010440).

References

Berger-Muller S, Suzuki T. Seven-pass transmembrane cadherins: roles and emerging mechanisms in axonal and dendritic patterning. Mol. Neurobiol. 2011; 44:313–320. [PubMed: 21909747]

Brenner S. The genetics of Caenorhabditis elegans. Genetics. 1974; 77:71–94. [PubMed: 4366476]

Chen PL, Clandinin TR. The cadherin *flamingo* mediates level-dependent interactions that guide photoreceptor target choice in Drosophila. Neuron. 2008; 58:26–33. [PubMed: 18400160]

Durbin, RM. PhD Thesis. University of Cambridge; 1987.

Fenstermaker AG, Prasad AA, Bechara A, Adolfs Y, Tissir F, Goffinet A, Zou Y, Pasterkamp RJ. Wnt/planar cell polarity signaling controls the anterior–posterior organization of monoaminergic axons in the brainstem. J. Neurosci. 2010; 30:16053–16064. [PubMed: 21106844]

Hall DH, Russell RL. The posterior nervous system of the nematode *Caenorhabditis elegans*: serial reconstruction of identified neurons and complete pattern of synaptic interactions. J. Neurosci. 1991; 11:1–22. [PubMed: 1986064]

Harterink M, Kim DH, Middelkoop TC, Doan TD, van Oudenaarden A, Korswagen HC. Neuroblast migration along the anteroposterior axis of *C. elegans* is controlled by opposing gradients of Wnts and a secreted frizzled-related protein. Development. 2011; 138:2915–2924. [PubMed: 21653614]

Hedgecock EM, Culotti JG, Hall DH. The unc-5, unc-6, and unc-40 genes guide circumferential migrations of pioneer axons and mesodermal cells on the epidermis in *C. elegans*. Neuron. 1990; 4:61–85. [PubMed: 2310575]

Hilliard MA, Bargmann CI. Wnt signals and frizzled activity orient anterior–posterior axon outgrowth in *C. elegans*. Dev. Cell. 2006; 10:379–390. [PubMed: 16516840]

Hutter H. Extracellular cues and pioneers act together to guide axons in the ventral cord of *C. elegans*. Development. 2003; 130:5307–5318. [PubMed: 13129845]

Kirszenblat L, Pattabiraman D, Hilliard MA. LIN-44/Wnt directs dendrite outgrowth through LIN-17/Frizzled in C. elegans neurons. PLoS Biol. 2011; 9:e1001157. [PubMed: 21949641]

Knobel KM, Jorgensen EM, Bastiani MJ. Growth cones stall and collapse during axon outgrowth in *Caenorhabditis elegans*. Development. 1999; 126:4489–4498. [PubMed: 10498684]

Korswagen HC. Canonical and non-canonical Wnt signaling pathways in *Caenorhabditis elegans*: variations on a common signaling theme. Bioessays. 2002; 24:801–810. [PubMed: 12210516]

Lee RC, Clandinin TR, Lee CH, Chen PL, Meinertzhagen IA, Zipursky SL. The protocadherin *Flamingo* is required for axon target selection in the *Drosophila* visual system. Nat. Neurosci. 2003; 6:557–563. [PubMed: 12754514]

Lyuksyutova AI, Lu CC, Milanesio N, King LA, Guo N, Wang Y, Nathans J, Tessier-Lavigne M, Zou Y. Anterior–posterior guidance of commissural axons by Wnt-frizzled signaling. Science. 2003; 302:1984–1988. [PubMed: 14671310]

Maro GS, Klassen MP, Shen K. A beta-catenin-dependent Wnt pathway mediates anteroposterior axon guidance in *C. elegans* motor neurons. PLoS ONE. 2009; 4:e4690. [PubMed: 19259273]

McIntire SL, Reimer RJ, Schuske K, Edwards RH, Jorgensen EM. Identification and characterization of the vesicular GABA transporter. Nature. 1997; 389:870–876. [PubMed: 9349821]

Najarro EH, Wong L, Zhen M, Carpio EP, Goncharov A, Garriga G, Lundquist EA, Jin Y, Ackley BD. *Caenorhabditis elegans flamingo cadherin fmi-1* regulates GABAergic neuronal development. J. Neurosci. 2012; 32:4196–4211. [PubMed: 22442082]

Norris AD, Lundquist EA. UNC-6/netrin and its receptors UNC-5 and UNC-40/DCC modulate growth cone protrusion in vivo in *C. elegans*. Development. 2011; 138:4433–4442. [PubMed: 21880785]

Pan CL, Howell JE, Clark SG, Hilliard M, Cordes S, Bargmann CI, Garriga G. Multiple Wnts and frizzled receptors regulate anteriorly directed cell and growth cone migrations in *Caenorhabditis elegans*. Dev. Cell. 2006; 10:367–377. [PubMed: 16516839]

Sanchez-Alvarez L, Visanuvimol J, McEwan A, Su A, Imai JH, Colavita A. VANG-1 and PRKL-1 cooperate to negatively regulate neurite formation in *Caenorhabditis elegans*. PLoS Genet. 2011; 7:e1002257. [PubMed: 21912529]

Senti KA, Usui T, Boucke K, Greber U, Uemura T, Dickson BJ. *Flamingo* regulates R8 axon–axon and axon–target interactions in the *Drosophila* visual system. Curr. Biol. 2003; 13:828–832. [PubMed: 12747830]

Shafer B, Onishi K, Lo C, Colakoglu G, Zou Y. Vangl2 promotes Wnt/planar cell polarity-like signaling by antagonizing Dvl1-mediated feedback inhibition in growth cone guidance. Dev. Cell. 2011; 20:177–191. [PubMed: 21316586]

Song S, Zhang B, Sun H, Li X, Xiang Y, Liu Z, Huang X, Ding M. A Wnt-Frz/Ror-Dsh pathway regulates neurite outgrowth in *Caenorhabditis elegans*. PLoS Genet. 2010; 6

Steimel A, Wong L, Najarro EH, Ackley BD, Garriga G, Hutter H. The Flamingo ortholog FMI-1 controls pioneer-dependent navigation of follower axons in *C. elegans*. Development. 2010; 137:3663–3673. [PubMed: 20876647]

Stringham E, Pujol N, Vandekerckhove J, Bogaert T. unc-53 controls longitudinal migration in *C. elegans*. Development. 2002; 129:3367–3379. [PubMed: 12091307]

Takeichi M. The cadherin superfamily in neuronal connections and interactions. Nat. Rev. Neurosci. 2007; 8:11–20. [PubMed: 17133224]

Wu M, Herman MA. A novel noncanonical Wnt pathway is involved in the regulation of the asymmetric B cell division in *C. elegans*. Dev. Biol. 2006; 293:316–329. [PubMed: 16631156]

Zhou HM, Walthall WW. UNC-55, an orphan nuclear hormone receptor, orchestrates synaptic specificity among two classes of motor neurons in *Caenorhabditis elegans*. J. Neurosci. 1998; 18:10438–10444. [PubMed: 9852581]

Zou Y. Navigating the anterior–posterior axis with Wnts. Neuron. 2006; 49:787–789. [PubMed: 16543126]

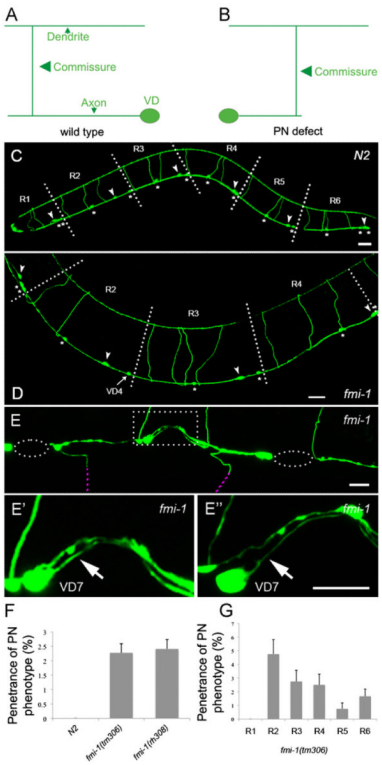

Fig. 1.

PN defects in *fmi-1* animals. ((A) and (B)) A cartoon of a VD neuron in *wt* (A) and *fmi-1* animals (B). (C) In *juIs76* animals, the D-type GABAergic neurons can be organized in six regions (R1–R6) along the A/P axis. Regions R1–R5 each contain one DD (arrowheads) and two VDs (asterisks) whereas region R6 contains one DD and three VDs. VD and DD commissures are positioned anterior to their respective cell body. (D) In this *fmi-1* animal, VD4 commissure is in region R3 instead of R2. As a result, R2 and R3 contain two and four commissures, respectively. In contrast, R2 and R3 in *wt* always contain three commissures as depicted (C). ((E)–(E')) Ventral view of another *fmi-1* animal where VD7 is displaying a PN (arrow). (E") Rotated version of (E'). (F) Quantification of the PN phenotype penetrance. (G) Quantification of the PN phenotype per region. Dashed ellipse indicates regions lacking neuronal processes in the VNC whereas purple dashed lines show commissures out of focus. Dashed square show region magnified and depicted in ((E')—(E")). Scale bar is 20 μm in ((C) and (D)) and 10 μm in ((E)–(E")). Anterior is to the left.

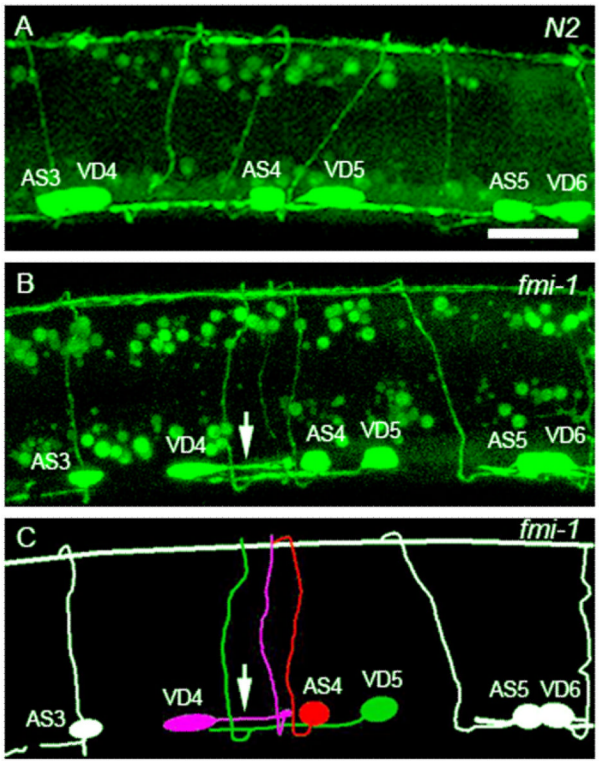

Fig. 2.

VD neurons display PN defects in *fmi-1;lhIs35* animals. (A) L2 *wt* animal expressing the *lhIs35* marker. VD neurons are posterior to AS neurons. (B) VD4 displaying a PN defect (arrow) in an L2 *fmi-1* animal. In spite of this defect, VD4 still projects a ventrodorsal commissure. VD5 has a normal AN. Note that VD6 commissure is not shown in the *fmi-1* animal. (C) A cartoon of (B). Scale bar is 10 μm.

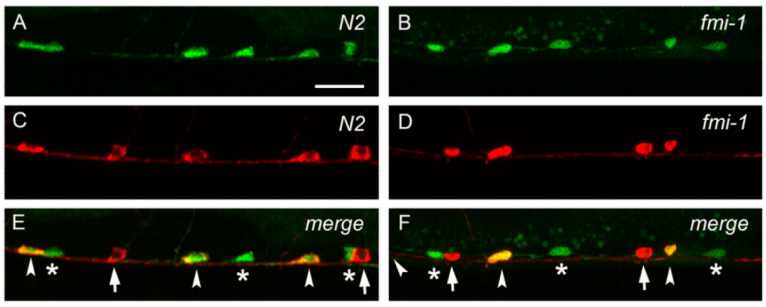

Fig. 3.

VD neurons are positioned posterior to AS neurons in wt and *fmi-1* animals. ((A) and (B)) *lhIs35* labels VD and AS neurons in *wt* (A) and *fmi-1* (B). ((C) and (D)) AS neurons are labeled by RFP (*Punc-53::tagRFP*) in *wt* (C) and *fmi-1* (D). ((E) and (F)) Merge views. VD neurons (asterisks) are located posterior to AS (arrowheads) in both backgrounds. Notice that the first AS neuron, from left to right, is not shown in (F). Red marker is also expressed in the DA neurons (arrows in E and F). Scale bar is 10 μm.

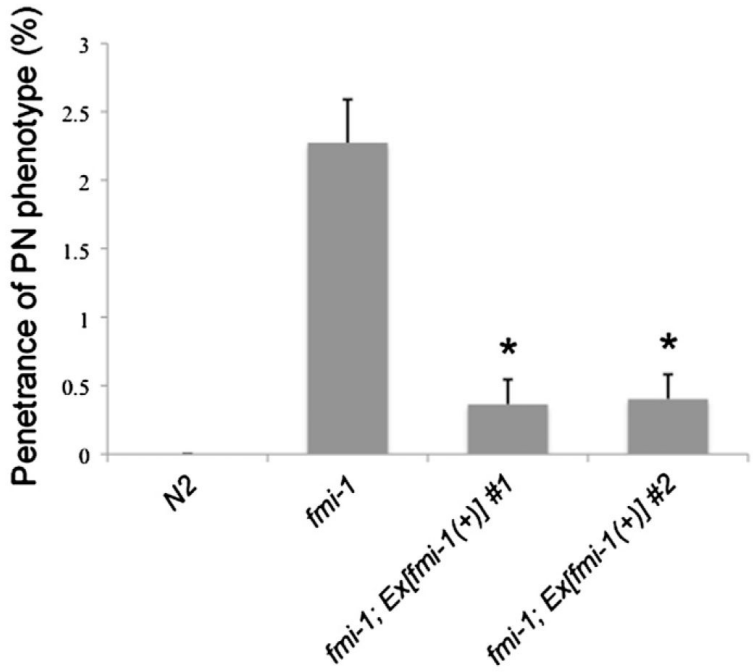

Fig. 4.

Transgenic rescue of PN defects in *fmi-1* adults. For each data set, *n* represents at least 1100 VDs. Asterisks indicates significantly different from *fmi-1* by χ^2 test, $p<0.05$.

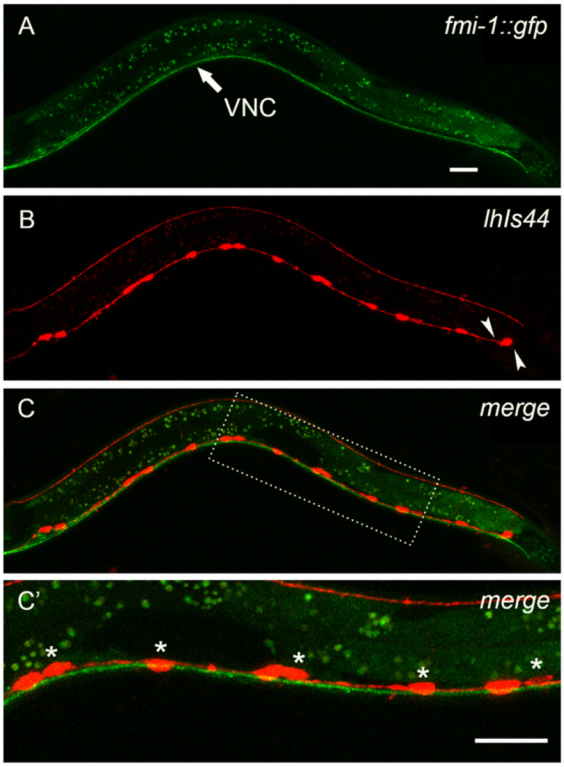

Fig. 5.

FMI-1 is in the VNC at early L2 stage during AN growth. (A) An early L2 *fmi-1* animal expressing a rescuing FMI-1::GFP. GFP-labeled FMI-1 is consistently present in the VNC. (B) The same animal coexpressing a red VD marker (*lhIs44*). Arrowheads indicate the future position of VD12 and VD13 which have yet to develop in this early L2 animal. ((C)–(C')) FMI-1::GFP is not detectable in the VD neurons but is present in neighboring axons in the VNC. Dashed rectangle show inset depicted in (C'). Asterisks indicate VD neurons. Scale bar is 10 μm.

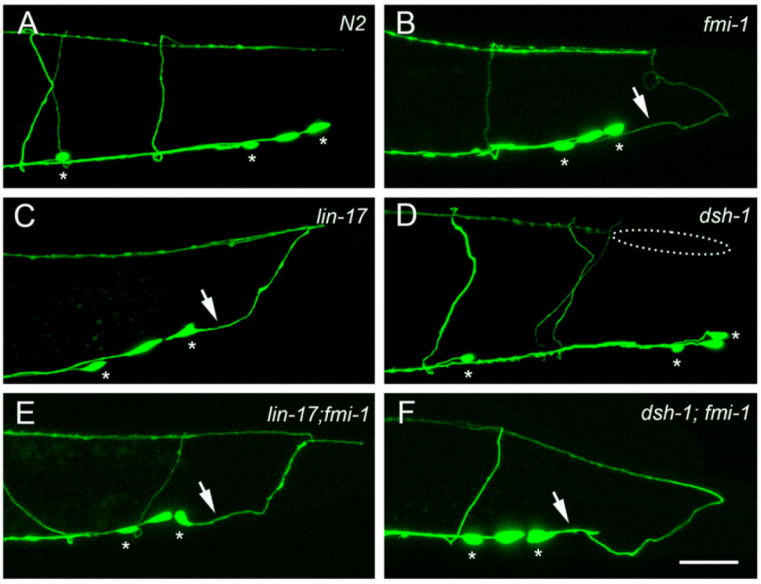

Fig. 6.

A/P neurite growth defects in *fmi-1, lin-17* and *dsh-1.* (A) Region R6 in *wt.* (B) An *fmi-1* animal displaying a PN phenotype in R6. (C) A *lin-17* animal displaying *fmi-1*-like defects in R6. (D) *dsh-1* animals display defects in dorsal neurite extension (dashed ellipse), but not PNs. PN defects are present in the *lin-17;fmi-1* (E) and *dsh-1;fmi-1* animals (F). Asterisks indicate VD neurons. Scale bar is 20 μm.

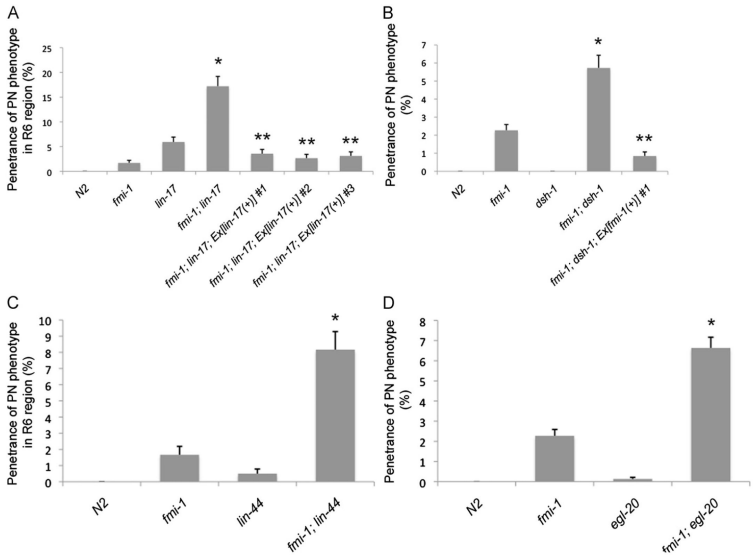

Fig. 7.

fmi-1 genetically interacts with *lin-17, dsh-1, lin-44 and egl-20*. (A) Quantification of the PN phenotype in region R6 in *lin-17* and *fmi-1* mutants and *lin-17;fmi-1* double mutants using *juIs76. lin-17* expression, under its endogenous promoter, rescues PN defects in *lin-17;fmi-1* double mutants (last three bars). (B) Penetrance of PN defects in regions R2–R6 in *dsh-1;fmi-1* double mutant animals. Defects were rescued by transgenic expression of *fmi-1* in the double mutants (last bar). PNs are not present in either *dsh-1 or N2* control animals. (*) indicates a significant increase in the penetrance of PN phenotype in double mutant animals compared to that of either single mutant (χ^2 test, $p<0.05$). (**) indicates a significant decrease in the penetrance of PN phenotype in the rescue line compared to that of the double mutant animal (χ^2 test, $p<0.05$).

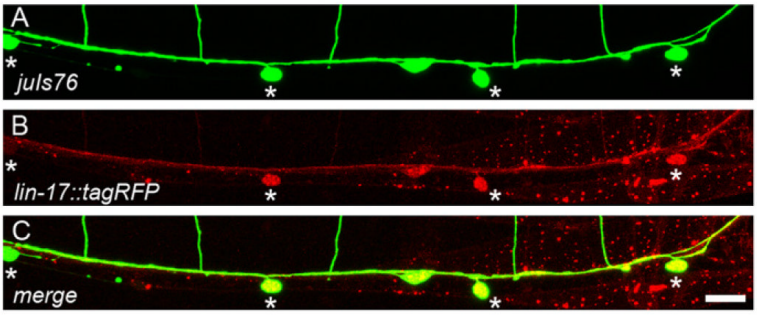

Fig. 8.

lin-17::tagRFP is expressed in VD. (A) Ventral view of an adult *juIs76* animal, DDs and VDs (asterisks) are green. (B) Same animal coexpressing *Plin-17::lin-17::tagRFP.* ((C) Colocalization (yellow) indicates LIN-17::tagRFP is present in the VD neurons. Scale bar is 10 μm.

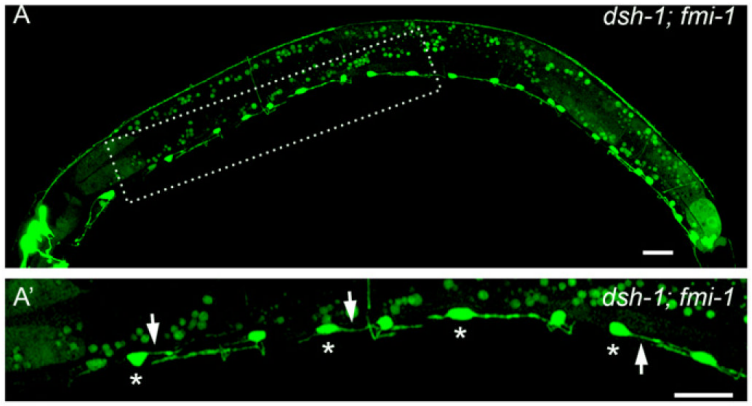

Fig. 9.

dsh-1 is an enhancer of *fmi-1.* ((A)–(A')) *dsh-1;fmi-1* double mutant animal displaying multiple PN defects in the VDs (asterisks). Arrows mark PN defects. Scale bar is 10 μm.

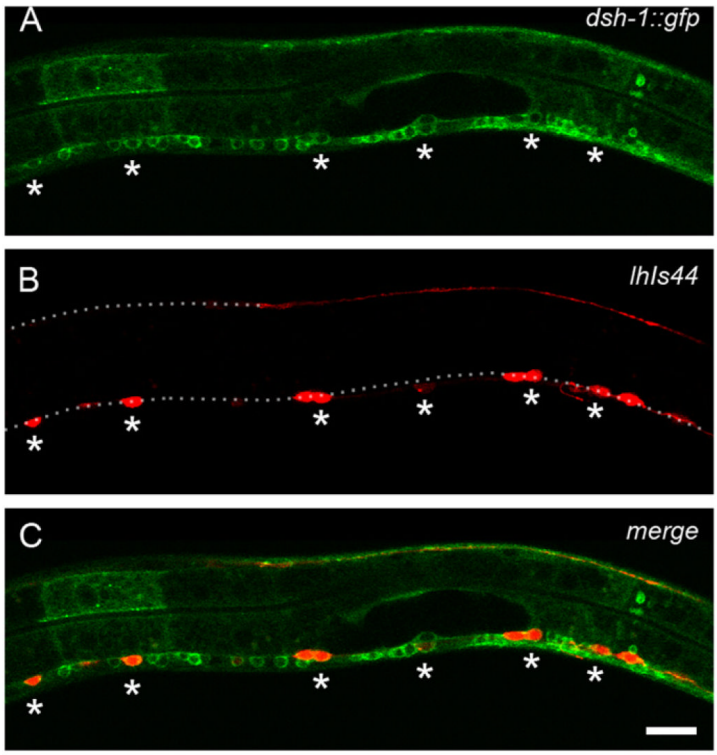

Fig. 10.

DSH-1::GFP is present in the VDs at early L2 stage. (A) *Pdsh-1::dsh-1::gfp* labels neurons along the VNC. (B) Same animal coexpressing a red GABAergic marker (*lhIs44*). (C) DSH-1::GFP is present in the VD neurons (asterisks). Yellow indicates colocalization. Dashed lines in (B) indicate the DNC and VNC. Scale bar is 10 μm.

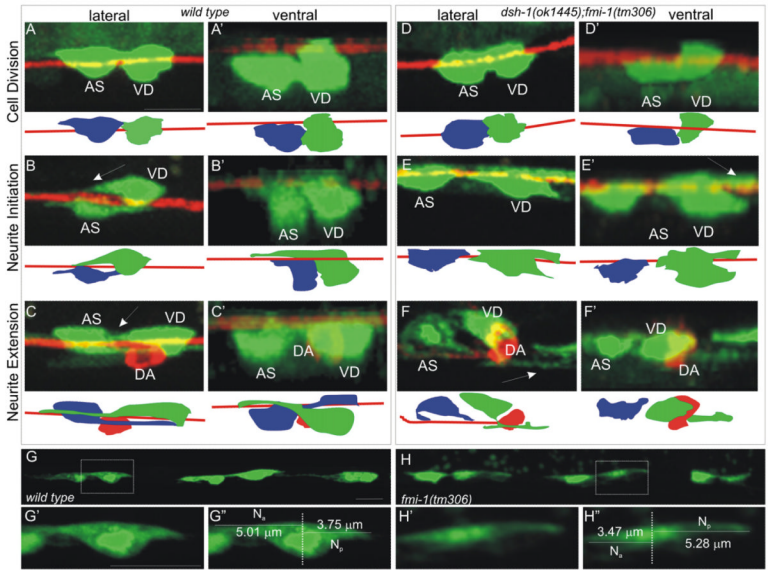

Fig. 11.

Early VD development. *lhIs35* (AS and VD neurons) and *Punc-53::tagRFP* (DA neurons) were visualized in *wt* and *dsh-1;fmi-1* mutants ((A)–(I)). In all panels anterior is to the left. Early VD development was classified into stages: cell division ((A) and (D)), neurite initiation ((B) and (E)) and neurite extension ((C) and (F)). No differences were found in cell division. However, during neurite initiation, at a time when cells were forming ANs ((B)—arrow), mutants more often formed posteriorly extended neurites ((E)—arrow). During neurite extension, at a time when wt VDs displayed an AN ((C)—arrow), we found PNs in mutant animals ((F)—arrow). For each panel we have provided a cartoon where VD (green), AS (blue) and VNC (red) are illustrated. ((G) and (H)) As the VDs flattened along the VNC, it was possible to observe anterior and posterior projections from the cells in wild-type (G) and *fmi-1(tm306)* (H). ((G') and (H')) Individual VD neurons (boxed regions–(G) and (H)). ((G") and (H")) We measured the anterior neurite length (Na) and posterior neurite length (Np). Scale bar is 5 μm.

Table 1

PN defects in animals using *lhIs35* marker.

Genotype	No. of animals	No. of VD neurons	VD1/VD2	Penetrance of the PN phenotype per cell type[a]									VD12/13	Penetrance[b]
				VD3	VD4	VD5	VD6	VD7	VD8	VD9	VD10	VD11		
lhIs35	50	450	N/D	0.00	0.00	0.00	0.00	0.00	0.00	0.00	0.00	0.00	N/D	0.00
lhIs36	53	477	N/D	0.00	0.00	0.00	0.00	0.00	0.00	0.00	0.00	0.00	N/D	0.00
fmi-1	52	468	N/D	0.00	7..69	3.85	3.85	11.54	13.46	3.85	3.85	0.00	N/D	5.34
lin-17	44	396	N/D	0.00	0.00	0.00	0.00	0.00	0.00	0.00	4.55	4.55	N/D	1.01
dsh-1	56	504	N/D	0.00	0.00	0.00	0.00	0.00	0.00	0.00	0.00	0.00	N/D	0.00
prkl-1 [c]	50	450	N/D	0.00	0.00	0.00	0.00	0.00	0.00	0.00	0.00	0.00	N/D	0.00
vang-1	51	459	N/D	0.00	0.00	0.00	0.00	0.00	0.00	0.00	0.00	0.00	N/D	0.00
dsh-1;fmi-1	60	540	N/D	13.33	33.33	13.33	13.33	6.67	6.67	8.33	10.00	1.67	N/D	11.85[d]

(N/D): not determined.

All numbers are in percentage.

[a] For example, number of defective VD3s/total number of VD3s scored.

[b] Total number of defective VDs/total number of VDs scored.

[c] *lhIs36* marker was used to score PN defects in these animals.

[d] Value different than *fmi-1* animals by X^2 test, $p<0.01$.

Table 2

Underextension defects or gaps in the VNC.

Genotype	No. of animals	No. of VD neurons	VD1/VD2	Penetrance of the neurite underextension defects per cell type[a]									VD12/13	Penetrance[b]
				VD3	VD4	VD5	VD6	VD7	VD8	VD9	VD10	VD11		
lhIs35	50	450	N/D	0.00	12.00	2.00	0.00	2.00	10.00	8.00	0.00	0.00	N/D	4.00
fmi-1	52	468	N/D	38.46	48.08	23.08	28.85	28.85	42.31	15.38	15.38	9.62	N/D	27.78
lin-17	44	396	N/D	4.55	11.36	4.55	0.00	4.55	20.45	11.36	15.91	9.09	N/D	9.09
dsh-1	56	504	N/D	17.86	19.64	12.50	17.86	17.86	7.14	7.14	10.71	5.36	N/D	12.90

(N/D) not determined.

All numbers are in percentage.

[a]For example, number of defective VD3s/total number of VD3s scored.

[b]Total number of defective VDs/total number of VDs scored.